Phosphorous-31 MAS NMR Studies of Insertion of Trialkylphosphine Oxides Into Transition Metal Open Framework Coordination Polymers

Adhyaru, B., UF, Chemistry
Woodward, J., UF, Chemistry
Bowers, C.R., UF, Chemistry
Talham, D.R., UF, Chemistry

The goal of this study was to demonstrate the insertion of a guest molecule, trialklyphosphine oxide probe (trimethylphosphine oxide [TMPO], triethylphosphine oxide [TEPO], tri-*n*-propyl-phosphine oxide [TPPO], and tri-*n*-butylphosphine oxide [TBPO]) into a host, two open framework coordination polymers, $[Ni(4,4'\text{-bipy})_3(H_2O)_2](4,4'\text{-bipy})_{1.4}(H_2O)_3(ClO_4)_2]$ and $[Co(4,4'\text{-bipy})_3(H_2O)_2](4,4'\text{-bipy})_{1.4}(H_2O)_3(ClO_4)_2]$. In the past, amines containing ^{13}C and ^{15}N have been used as probes and their insertion into a host was monitored by solid state magic angle spinning (MAS) NMR spectroscopy.

Recently, work has focused on the use of phosphines and phosphine oxides as probes to characterize acid sites in zeolites, silica-alumina, and other similar materials using ^{31}P NMR. In order to gain information about acid/base sites within the host framework after the insertion, a series of ^{31}P MAS NMR spectra were obtained for the dry probe molecules and after the addition of 100 μL of water. In all cases, a noticeable shift downfield after the addition of water was observed and interpreted as the phosphine oxide hydrogen bonding to the solvent. Single crystals of the framework structures were prepared by the combination of one equivalent of $M(ClO_4)_2 \cdot 6H_2O$ (M=Ni, Co) with three equivalents of 4,4'-bipy, under hydrothermal conditions and characterized by single crystal x-ray diffraction. Insertion of the probe molecule involved mixing one equivalent of the powdered framework and phosphine oxide in a hexane solution. Gas chromatography revealed that insertion of the probe molecule displaces 4,4'-bipy guest molecules already present within the framework, and as the length of the alkyl chain of the phosphine oxide increases, a smaller quantity is taken into the host.

The ^{31}P MAS NMR experiments were utilized to study the interactions of the basic probe molecule with acidic sites (metal coordinated water molecules) on the host. Assignments of the resonances are based on similar work, employing trialkylphosphine oxide probing acid sites on zeolites and silica-alumina.[1] For the Ni framework inserted with TMPO, two distinct peaks were observed and assigned as Bronsted acid sites (downfield resonance) and Lewis acid sites (upfield resonance); whereas, only one peak was observed for the other three probe molecules and assigned as Lewis acid sites. In the Co framework samples, the MAS NMR spectrum was dominated by a paramagnetic interaction leading to very broad resonances, a noticeable difference between the two framework polymers. X-ray powder diffraction experiments indicate the insertion is non-topotactic, and a significant loss of crystallinity is observed, an expected result. Although the NMR experiments reveal how the probe molecule interacts with the host, the structural changes within the framework due to this insertion are not clear.

[1] Baltusis, L., *et al.,* J. Am. Chem. Soc., **108,** 7119-7120 (1986).

Solid State Carbon-13 CP/MAS-NMR Spectroscopy of Natural and Synthetic Melanins

Adhyaru, B., UF, Chemistry
Akhmedov, N., UF, Chemistry
Denisenko, S., UF, Chemistry
Bowers, C.R., UF, Chemistry
Katritzky, A., UF, Chemistry

Melanin, a pigment found in most animals, has a complex chemical structure. Determining information about the chemical structure of melanin may provide insight into biological mechanisms of skin-related

diseases such as melanoma as well as applications in the cosmetic industry. The problem that exists in studying this molecule is its insolubility in common organic solvents. Due to this factor, we have employed solid state ^{13}C NMR techniques.

Because melanin is a heterogenous polymer, we first obtained ^{13}C CP/MAS and non-quarternary carbon suppression spectra for model compounds (dopamine, L-dopa, 5,6-dimethoxy-2-indole carboxylate, and a pyrrole compound). The linewidths of the various peaks were on the order of 30 to 40 Hz and the spectra were easily assigned. Next, ^{13}C CP/MAS spectra were obtained for three melanin compounds, melanin obtained from *Sepia officinalis*, *Sepia officinalis* (free acid), and human hair. A large amount of signal averaging (10,000 scans) was required to obtain a spectrum. The peaks observed were relatively broad due to polymerization and possible paramagnetic indole units within the polymer. However, three basic chemical shift ranges were observed and include the following: aliphatic carbon atoms (20 to 60 ppm), indole/aromatic carbon atoms (100 to 140 ppm), carboxyl carbon atoms (160 to 180 ppm).

There was also a considerable difference between the spectra. The Sepia melanin spectra displayed more aromatic/indole and carboxyl functionalities, whereas, the human hair displayed more aliphatic functionality and very little aromatic functionality. This may be a result of the different synthetic pathways for the melanin samples. In order to extract more information from these broad spectra, we are applying various decoupling schemes and correlation spectroscopy where we would be able to differentiate between CH, CH_2, CH_3, and quaternary carbon atoms.

Methylaluminoxane Structure Analysis: Frequency-Stepped, Field Swept, and High-Field MAS ^{27}Al NMR and Comparison with EFG Tensors from *ab initio* Molecular Orbital Calculations

Bryant, P.L., Louisiana State Univ., Chemistry
Mrse, A.A., LSU, Chemistry
Emery, E.F., LSU, Chemistry
Butler, L.G., LSU, Chemistry
Harwell, C.R., LSU, Chemistry
Hall, R.W., LSU, Chemistry
Simeral, L.S., Albemarle Corporation
Caldwell, T., NHMFL
Reyes, A.P., NHMFL
Kuhns, P., NHMFL
Gan, Z., NHMFL

The structure of methyl aluminoxane (MAO) is unknown. It may be a dynamic mixture of linear, ring, and cage complexes, all formed from methyl aluminum oxane subunits (CH_3AlO) during the controlled hydrolysis of trimethylaluminum. A knowledge of the MAO structure is important for the continued development of new-generation polyolefin catalysts. In this work, we pursue a two-prong investigation. First, we seek a reliable ^{27}Al NMR spectrum of MAO. Second, molecular aluminum clusters analogous to proposed MAO units are studied, both experimentally with ^{27}Al NMR and with molecular orbital calculations to generate ^{27}Al NMR parameters. Then, the validated MO methods are used to predict ^{27}Al NMR spectra for proposed structures, and the calculated spectra are compared with the best available experimental spectra.

The upper and lower bounds for the ^{27}Al Quadrupolar Coupling Constant, Cq, in MAO determined in this work add new interest in the use of MAS probes in resistive and hybrid magnet systems. Those fields of 33 and 45 T, when combined with 20 to 40 kHz spin rates, now seem to offer an excellent chance of success for resolving the longstanding structural questions associated with MAO.

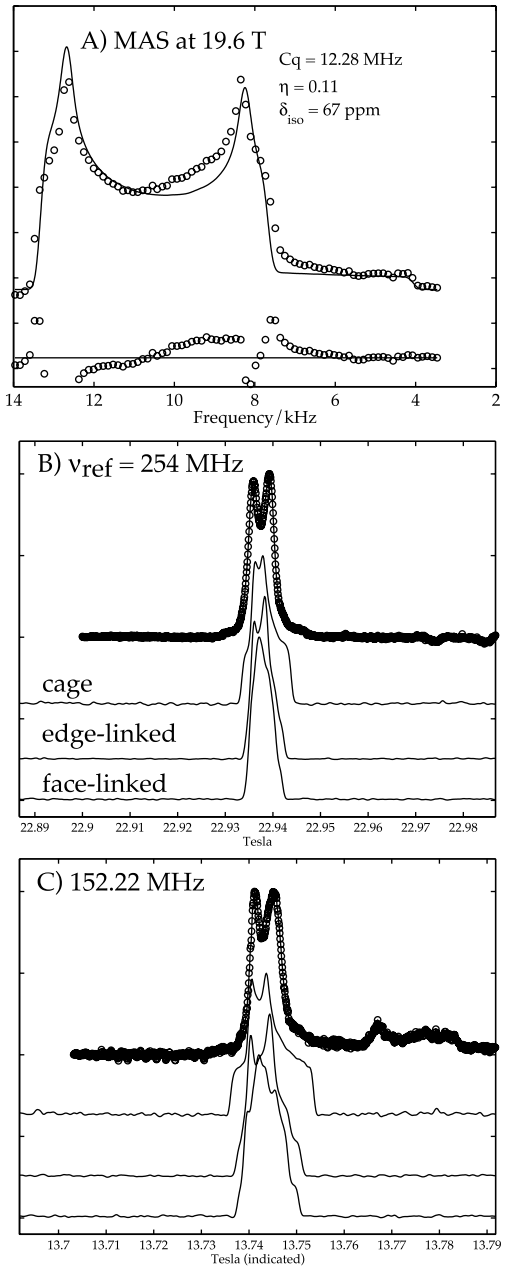

Figure 1. (A) 27Al MAS NMR at 19.6 T (833 MHz 1H) of an isopropoxide tetraaluminum complex. (B), (C) Field-swept 27Al NMR of MAO. Below each spectrum are shown simulated 27Al NMR spectra for three postulated structural components of MAO.

Acknowledgments: The support of the National Science Foundation, CHE-9977124, is gratefully acknowledged (LGB, RWH, LSS), as is funding for NMR and computer cluster equipment from the Louisiana Board of Regents.

High Frequency and High Field Electron Paramagnetic Resonance Studies of Ferrate Species

Burnett, C.R., Florida Institute of Technology, Chemistry
Smith, T., FIT, Chemistry
Saylor, C.A., NHMFL
van Tol, J., NHMFL
Sharma, V., FIT, Chemistry

Fe(VI) is a d^2, triplet with a spin, S=1. Although conventional EPR spectroscopic methods have been employed on a solid sample of potassium ferrate(VI), the additional research at the NHMFL will be the first attempt to determine the structural and electronic environments of Fe(VI) in an aqueous solution. High frequency and high field EPR techniques have proven more effective in elucidating the electronic structures of species. The combination of multi-frequency (25 to 3000 GHz, 100 cm^{-1}) and high field, with the ability to perform continuous fields sweeps over a broad range, (0 to 17 T) allow the EPR spectrometer to chose a convenient parameter "window" to observe most of the multitude of transitions characterizing the species. EPR studies at high frequency and high field of a potassium ferrate(VI) crystal over a wide temperature range (4 to 298 K) were conducted. The EPR spectra of a potassium ferrate(VI) crystal suggest exchange interactions that were not seen before using conventional EPR techniques. The overall aim of this study is to obtain further insight into the properties of Fe-O bond, energy level patterns of the ion, electronic transition, and coupling reactions.

Measurements with other ferrate(VI) (barium, strontium, rubidium, and cesium) will be performed to see the effect of cations on the electronic environment of Fe(VI) species. Ferrates(VI) will be prepared by a wet chemistry method. EPR spectra of frozen aqueous solution of Fe(VI) are also planned. For aqueous Fe(VI) spectra, the samples will be prepared by adding solid K_2FeO_4

into borate/phosphate (pH 9.0) buffer solution. At this pH, Fe(VI) species is stable to perform the experiments.

Preliminary Orientational and Structural Studies of Antimicrobial Salivary Histatin-5 in Oriented Lipid Bilayers

Cotten, M., Univ. of Washington, Chemistry
Drobny, G.P., Univ. of Washington, Chemistry
Stayton, P.S., Univ. of Washington, Bioengineering

Much interest has grown for histatin-5 (hsn5), one of the multifunctional histidine-rich histatins found in human saliva. This 24-amino-acids long polypeptide (DSHAKRHHGYKRKFHEKHHSHRGY) is cationic under normal physiological conditions (pH 7.4). It binds to teeth and regulates the formation of enamel,[1] a function commonly and efficiently performed by acidic proteins.[3] Its antimicrobial activity has been the subject of many studies as well. The peptide is unstructured in aqueous solution.[5] However, CD spectra of the peptide in the presence of DMPC bilayers suggest that the global structure of its C-16 fragment (amino acids 9 to 24, "C16-hsn5") has some α-helical character.[6] In addition, it has been suggested that hsn5 interacts with the negatively charged lipids in the membranes of its targets.[4]

Interestingly, both mineral and lipid surfaces contain negatively charged phosphate groups, so one may ask whether the peptide interacts with these surfaces in a similar fashion, thereby allowing different functions to be performed by similar conformational states. Some insights into these questions, as well as into the selectivity and mechanisms of multiple actions of the full-length peptide, require some elementary information, including its local secondary structure, its interactions, and points of contact with the surfaces. Here, solid state NMR has been used in the early steps of this investigation to study the peptide in a lipidic environment. Preliminary data to determine whether the peptide adopts a unique orientation with respect to the lipid bilayer have been obtained. Specifics about the technique have been derived from some elegant static solid-state NMR structural studies, which have utilized oriented samples to study a variety of labeled peptides and proteins associated with lipid bilayers.[7]

^{15}N Phe$_{14}$ hsn5 and ^{15}N Phe$_{6}$ C-16-hsn5 were synthesized by solid phase synthesis using Fmoc chemistry, purified by HPLC, and characterized by mass spectroscopy. The peptides were then incorporated in uniformly oriented and hydrated lipid bilayers consisting of a mixture of negatively-charged phosphoglycerol (10% DMPG) and neutral phosphocholine (90 % DMPC). The samples were oriented between glass plates using a peptide to lipid ratio of 1 to 20. The ^{15}N spectrum of ^{15}N Phe$_{6}$ C-16-hsn5 and ^{15}N Phe$_{14}$ hsn5 in these oriented phospholid bilayers recorded at room temperature with the bilayer normal parallel to the applied static magnetic field are displayed in Fig. 1A and B, respectively. The 14 T wide-bore magnet equipped with a doubly (^{1}H and ^{15}N) tuned probe with a square coil of geometry suitable to fit the stacked glass plates of oriented samples was used to perform "ramped cross polarization" experiments on these samples.

Compared to the broad ^{15}N powder pattern for the peptide in the dry lipid mixture (Fig. 1C), a relatively sharp resonance centered around 70 ppm was observed for both the C-16 fragment and the full length peptide in the oriented lipid bilayers. Since this resonance is away from the isotropic chemical shift typically of about 100 ppm for amide nitrogens, this result strongly suggested that the peptides were not in the isotropic aqueous phase, but were rather interacting with the bilayer in a specific fashion. In other words, in the presence of lipids, hsn5 and its fragment adopt a given orientation with respect to the lipid bilayer and become motionally constrained. However, difficulties in obtaining the ^{15}N spectrum from the oriented samples were assigned to the low cross-polarization efficiency characteristic of nuclei undergoing motions. This indicated that the bilayer-interacting peptides were still experiencing some degree of motional freedom. The ^{15}N resonances from the oriented samples are in the low ppm range of the powder pattern. Under the conditions that the peptide is a-helical as previously documented by CD,[6] this information indicated that the peptides were oriented

perpendicular to the magnetic field and hence the bilayer normal. Therefore, the results are consistent with hsn5 and its C-16 fragment lying in the plane of the bilayer surface.

The sensitivity of ^{31}P chemical shifts interactions to the physical state of the lipids is a complementary tool, which can pinpoint possible defects caused by an antimicrobial peptide. However, ^{31}P spectra of the samples used to record the data shown in Fig. 1-A and B do not indicate substantial changes from the typical pattern observed for the peptide-free lipid bilayers. The pKA of the numerous histidine side chains being close to physiological pH, the impact of the pH, as well as the charge and content of the lipids on the lipid/hsn5 interactions and orientation of the peptide in the bilayers, are important considerations for future studies aiming at understanding the onslaught and determinants of biological activity. A transmembrane orientation will favor a mechanism of action by pore formation. On the other hand, if no transmembrane orientation is observed while (a) new lipid phase(s) appear(s), this may indicate a mechanism through induction of bilayer defects.

To further address questions about the dynamics, secondary structure and orientation of hsn5 in lipid bilayers, CP and PISEMA experiments on a series of specifically ^{15}N-labeled hsn5 in hydrated bilayers with variable sample conditions (pH, lipid type and content, exposure to D2O)[8] are well-indicated now that the peptide has been shown to have a propensity to orient specifically in lipid bilayers. Overall, the conformational study of histatin-5 will provide unique information that will be used to better understand the multifunctionality and mechanisms of action of this salivary peptide.

Acknowledgements: The authors are very grateful to Dr. Tim Cross (NHMFL), Dr. Riqiang Fu (NHMFL), Changlin Tian (NHMFL), and Nathan Oyler (University of Washington) for their precious help and discussion.

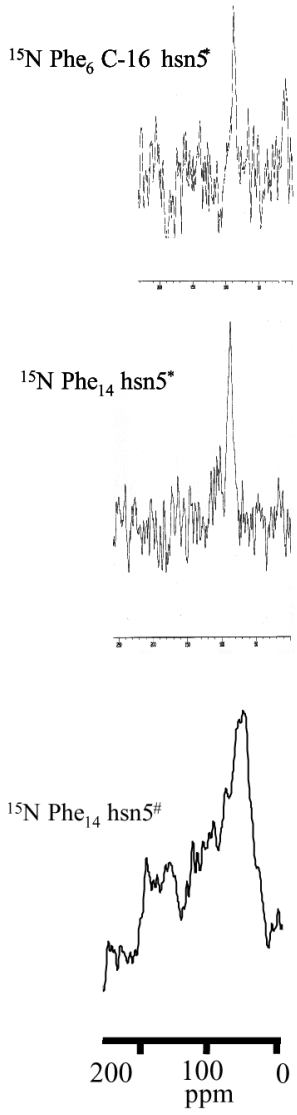

Figure 1. A and B are spectra from oriented and hydrated samples recorded in the NHMFL on the 600 MHz wide bore. The samples were oriented between glass plates. A: ^{15}N Phe$_6$ C-16-hsn5, B: ^{15}N Phe$_{14}$ Hsn5. C: Unoriented ^{15}N Phe$_{14}$ hsn5 in an unoriented and lyophilized lipid mixture. This data was collected at the University of Washington. All samples were made using a peptide to lipid ratio used of 1 to 20. The lipid mixture consisted of DMPC (90%) and DMPG (10%). The spectra were recorded at room temperature with cross polarization technique (Resonance frequencies: *60.8 MHz, #40.5 MHz).

[1] Hay, D., Arch. Oral. Biol., 20553-558 (1975); Oppenheim, F.G., *et al.,* J. Biol. Chem., **261,** 1177-1182 (1986).

[2] Tsai , H., *et al.,* Crit. Rev. Oral Biol. Med., **9**, 480-497 (1998).

[3] Lamkin, M.S., *et al.,* J. Dent. Res., **75**, 803-808 (1996).

[4] Pollock, J.J., *et al.,* Infect. Immun., **44**, 702-707 (1984); Oppenheim, F.G., Clinical Chemistry in Human Saliva., **1**, 151-160 (J. Tunuovo, Ed), CRC Press, FL. (1989).
[5] Raj, P.A., *et al.,* Biopolymers., **45**, 51-67 (1998).
[6] Raj , P.A., *et al.,* J. Biol. Chem., **269**, 9610-9619 (1994).
[7] Bechinger, B., *et al.,* J. Biomol. NMR., **1**, 167-173 (1991); Bechinger, B., *et al.,* Protein Science, **2**, 2077-2084 (1993). Bechinger, B., J. Mol. Biol., **263**, 768-775 (1996); Cross, T.A., *et al.,* Curr. Opin. in Struct. Biol. **4**, 574-581 (1994); Shon, K.-J., *et al.,* Science., **252**, 1303-1305 (1991); Ketchem, R.R., *et al.,* Structure, **5**, 1650-1669 (1997); McDonnell, P.A, *et al.,* J. Mol. Biol. **233**, 447-463 (1993); and Opella, S.J., Nat. Struct. Biol. NMR supplement, 845-848 (1997).
[8] Cotten, M., *et al.,* Biophys. J., **76**, 1179-1189 (1999).

^{1}H NMR Studies of a Zn(II)-Dependent Deoxyribozyme Following Paramagnetic Ion Replacement

Epperson, J., FSU, Chemistry
Greenbaum, N.L., FSU, Chemistry

For over four decades, Co(II) has been routinely used as a probe to investigate the metal binding environments of spectroscopically "silent" Zn(II) metalloproteins. The similar size, coordination chemistry, and ligand preferences between Zn(II) and Co(II), and the rich physical properties of the latter led to the widespread replacement of Zn(II) by Co(II) in both electronic and NMR physical studies of metalloproteins. Like metalloproteins, most nucleic acid-based enzymes require metal ions for catalytic activity, either through facilitation of the folding of DNA and RNA into stable tertiary structures, or through direct participation in the chemical reaction. Nucleic acid enzymes generally prefer alkaline earth metals, and as a result, transition metals like Co(II) have been largely ignored. However, a Zn(II)-dependent RNA-cleaving deoxyribozyme was recently identified through an *in vitro* selection process that favors tight binding to transition metal ions. In these ^{1}H NMR studies, we use Co(II) as a shift reagent to investigate the metal binding site structure of this new Zn(II)-dependent deoxyribozyme.

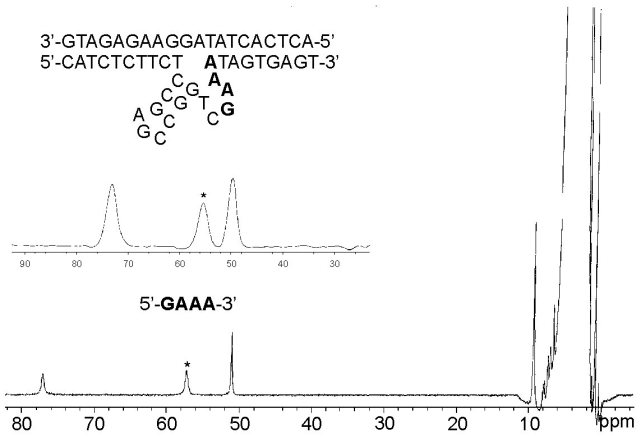

Figure 1. The ^{1}H NMR spectra (400 MHz at 25 °C) of Co(II)-RNA-cleaving deoxyribozyme (top inset) and Co(II)-dGAAA (bottom spectrum). Both samples were prepared at 2 mM nucleic acid/2 mM Co(II) in 10 mM Hepes buffer at pH 7.0. Asterisks indicate solvent exchangeable signals.

Three downfield hyperfine shifted signals were detected at 73 (T_1=20.3 ms), 55 (14 ms), and 50 (197 ms) ppm in addition to several smaller shifts (not shown) in the diamagnetic region of the spectrum for the 1:1 Co(II)-RNA-cleaving deoxyribozyme (see Fig. 1 inset). The sharpness of the signals and the relatively long T_1 values suggest a 5 or 6 coordinate metal geometry. The signal at 55 ppm is solvent exchangeable. The spectral shifts were almost identical to those seen for a 1:1 complex of Co(II) with a dGAAA tetranucleotide (see Fig. 1), suggesting that the Co(II) may be binding to the corresponding sequence within the deoxyribozyme. Future 2D NMR studies and an analysis of several deoxyribozyme mutants should help to confirm this analysis.

Determination of Relative Ordering of Activation Energy for Gas-Phase Ion Unimolecular Dissociation by Multiphoton Infrared Irradiation

Freitas, M.A., NHMFL
Hendrickson, C.L., NHMFL
Marshall, A.G., NHMFL/FSU, Chemistry

We report the use of a continuous wave CO_2 laser for the determination of relative activation energy for

unimolecular dissociation of large biomolecular ions. The $[M + 5H]^{5+}$ and $[M + 11H]^{11+}$ ions of bovine ubiquitin and the $[M + H]^{+}$ ion of bradykinin are irradiated with a CW CO_2 laser and the rate constant for dissociation at each of several laser intensities recorded. A plot of the natural logarithm of the first-order rate constant vs. the natural logarithm of laser intensity yields a straight line whose slope provides an approximate measure of the activation energy (E_a) for dissociation. For dissociation of protonated bradykinin, the absolute E_a value from infrared multiphoton dissociation (IRMPD) agrees with that obtained by blackbody infrared radiative dissociation (BIRD), whereas the IRMPD-determined E_a's for dissociation of the 5+ and 11+ charge states of bovine ubiquitin are lower than those obtained by BIRD. The relative E_a values for the 5+ and 11+ charge states of bovine ubiquitin from both BIRD and IRMPD are in good agreement. Master equation modeling was carried out on the model peptide, $(AlaGly)_8$, to characterize the nature of the internal energy distribution produced from irradiation by a monochromatic IR source (e.g. CW CO_2 laser) vs. a broadband IR source (e.g. blackbody). The master equation simulation shows that the internal energy distribution produced by irradiation with the CO_2 laser is essentially identical to that obtained by blackbody irradiation. Our combined experimental and theoretical results justify the IRMPD technique as a viable method for the determination of relative ordering of activation energies for dissociation of large (>50 atoms) ions.

Acknowledgements: We thank John P. Quinn, Daniel McIntosh, and Fei He (NHMFL), Scott McLuckey (Oak Ridge National Laboratory), Robert Dunbar (Case Western Reserve), and William Price (Marshall University) for their technical expertise and helpful discussion. This work was supported by NSF (CHE-93-22824), the NSF National High Field FT-ICR Facility (CHE-94-13008, CHE 99-09502), FSU, and the NHMFL.

[1] Freitas, M.A., *et al*., J. Am. Chem. Soc., **122**, 7768-7775 (2000).

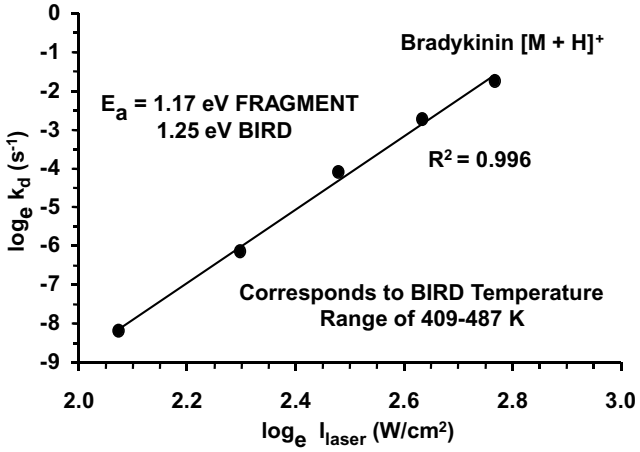

Figure 1. Plot of the natural logarithm of the first-order unimolecular dissociation rate constant, k_d, vs. the natural logarithm of laser intensity for protonated bradykinin. The activation energy for dissociation, E_a, is obtained from the slope of this line. Note the close agreement between the present IRMPD E_a value and that obtained previously by BIRD.

Weighted Quasi-Newton and Variable-Order, Variable-Step Adams Algorithm for Determining Site-Specific Reaction Rate Constants

He, F., NHMFL
Marshall, A.G., NHMFL/FSU, Chemistry

A weighted quasi-Newton algorithm for function minimization and a variable-order, variable-step Adams algorithm for ordinary differential equations were combined to solve site-specific gas-phase reaction rate constants. If the systems appear to be "stiff", smaller steps were taken in Adams method to search for the solution. A user supplied error tolerance was used to determine the accuracy of the solution. Upon the return of each solution, a weighted algorithm is introduced into the calculation of X^2 to minimize interference from noise. Lower and upper bounds for reagent fraction and rate constants were applied to ensure the validity of the results. The search direction is calculated by quasi-Newton algorithm. When a saddle point is suspected, a local search is carried out with a view to moving away from the saddle point. The information obtained from site-specific rate constants may provide further

insight into the reaction mechanism as well as gas-phase structure. It can be applied to gas-phase H/D exchange, deprotonation and other reactions (see Fig. 1).

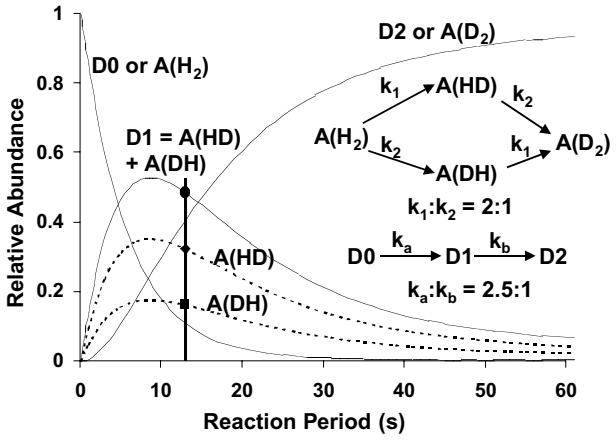

Figure 1. Concentration vs. reaction period for all four species, AH_2, AHD, AHD, and AD_2, in a system of two successive H/D replacement reactions (slightly different rate constants) for which the intermediate products formed after one step are chemically indistinguishable. Site-specific kinetic analysis (see below) yields the true individual rate constants, k_1 and k_2 As shown by the filled circles at a particular reaction period, the concentration, [D0], of molecules containing a total of 1 deuterium is the sum of the concentrations of species in which the hydrogen at the first or second site is replaced by deuterium.

Acknowledgements: The authors thank Dr. M. Kirk Green for helpful discussions, and Dr. Michael A. Freitas for helpful suggestions. This work was supported by grants from the NSF National High Field FT-ICR Mass Spectrometry Facility (CHE-94-13008), NIH(GM-31683), FSU, and the NHMFL.

[1] He, F., *et al*., J. Phys. Chem. A, **104**, 562-567 (2000).

Investigations of Manganese(III) Corrole Complexes as Solids and in Glasses

Krzystek, J., NHMFL
Telser, J., Roosevelt Univ., Chemistry
Hoffman, B.M., Northwestern Univ., Chemistry
Brunel, L.-C., NHMFL
Licoccia, S., Univ. of Rome Tor Vergata, Italy, Chemistry Science and Technology

The corroles are tetrapyrroles and analogues of both porphyrins and corrins, characterized by a direct link between two of the pyrrole rings. They have revealed some very interesting properties such as, the capability of maintaining a planar conformation even when completely substituted at the peripheral positions.[1] By having three amino-like nitrogen atoms, a corrole behaves as a trianionic ligand and may either stabilize high oxidation states for coordinated transition metal ions, or be easily oxidized to a cation radical itself, the latter being the most common situation in solution.[2]

While metalloporhyrins have been extensively studied by EPR and other spectroscopic techniques,[3] much fewer studies on the corresponding metal corroles exist in the literature.[4] Because of the similar ring structure of these two macrocycles, as well as the similarity of the corrole ring to the biologically relevant corrins, it is important to further characterize the metal complexes of corroles by magnetic resonance techniques.

An intriguing problem in corroles is the oxidation state of the central ion. It has been postulated[5] that due to a charge transfer, the nominal oxidation state of manganese (III) in porphyrins (and possibly in corroles) is in fact 2+, and this metal reduction is compensated by oxidation of the ring to a radical cation. We have previously confirmed by HFEPR,[6] that in the solid (8,12-diethyl-2,3,7,13,17,18-hexamethylcorrolato)manganese (complex **1**), the oxidation state is indeed 3+, resulting in a S=2 spin state; we characterized that state. Currently, we are reporting experiments in pyridine frozen solution.

A characteristic HFEPR spectrum of complex **1** in pyridine glass is shown in Fig. 1. The solid line is from the experiment, while the broken line is from a simulation using the following spin Hamiltonian parameters: S=2, D=-2.78 cm^{-1}, E=+0.03 cm^{-1}, g_x=g_y=g_z=2.00. This shows that even in solution the manganese ion exists in its 3+, high-spin state. Compared to the solid, $|D|$ increases by about 5%, and $|E|$ increases by about 50%; phenomena that can be attributed to axial coordination by pyridine molecule(s).

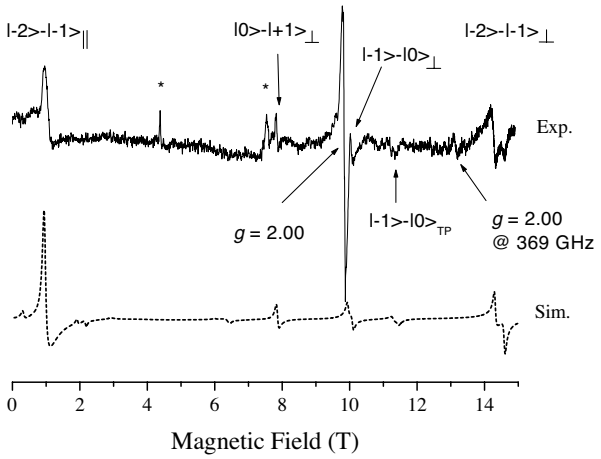

Figure 1. A 276.62 GHz EPR spectrum of a frozen pyridine solution of complex **1** at T=4.2 K (top) and its simulation (bottom). The spin Hamiltonian parameters used in simulation are in the text. The particular transitions in the powder pattern are identified and labeled accordingly. "TP" stands for an off-axis turning point. The two lines marked with asterisks originate from solid molecular oxygen present in the probe area or in the solution.

In a fresh solution, most of manganese exists in its Mn^{3+}, S=2, form, however, there is also a noticeable concentration of a Kramers-type species producing a strong g=2.00 signal. This signal is shown in narrow-sweep conditions in Fig. 2; its intensity increases with time at the expense of the Mn^{3+} signals. The hyperfine pattern allows its attribution to Mn^{2+}; however, its spin state is still under discussion since an independent susceptibility study does not agree with the usual S=5/2 for Mn^{2+}. Our current hypothesis is that the Mn^{2+} is intermediate-spin, i.e. S=3/2. The origin of the broad sidebands of the central hyperfine sextet in its HFEPR spectrum is under investigation. The sidebands are not observable in low-frequency conditions (X- and Q-band) and could arise from either (a) the zero-field splitting of the S=3/2 state, or (b) the compensating radical ion. It is clear, however, that no magnetic coupling between the Mn ion and the radical ion has been observed experimentally.

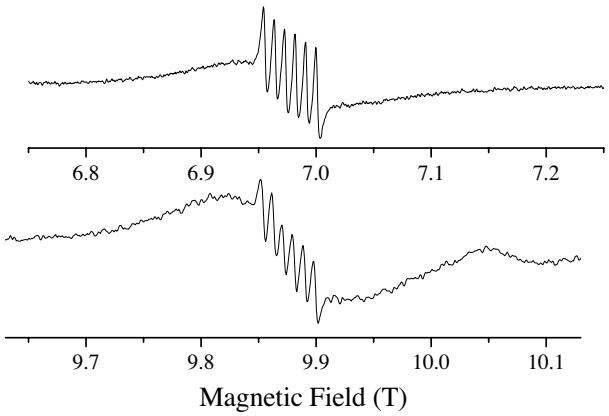

Figure 2. The g=2 region of the EPR spectra of a frozen pyridine solution of complex **1** at 195.48 GHz (top) and 276.62 GHz (bottom) at T=10 K. The central hyperfine sextet originates from Mn^{2+}. The origin of the broad sidebands is discussed in the text. The signal at 10.75 T, at 276.62 GHz, originates from S=2 Mn^{3+}.

1 Licoccia, S., *et al.*, Structure and Bonding, **84**, 73 (1995).
2 Cai, S., *et al.*, Inorg. Chem., **39**, 3466 (2000).
3 Walker, F.A., *et al.*, *Biological Magnetic Resonance*, ed. L.J. Berliner (Plenum Press, 1993) pp. 133-274.
4 Bendix, J., *et al.,* Chem. Commun., 1957 (2000).
5 Turner, P., *et. al.,* Inorg. Chem., **33**, 1406 (1994).
6 Krzystek, J., *et al., 1999 NHMFL Annual Research Review*.

Theoretical Maximal Precision for Mass-to-Charge Ratio, Amplitude, and Width Measurement in Ion-Counting (e.g., Time-of-Flight) Mass Analyzers

Lee, H.-N., NHMFL
Marshall, A.G., NHMFL/FSU, Chemistry

A theory previously developed for spectra with detector-limited (i.e., signal-independent) Gaussian-distributed noise is applied to calculate the maximal precision with which mass spectral peak parameters (mass-to-charge ratio, amplitude, width) can be determined from a discrete spectrum with source-limited Poisson-distributed noise. The precision depends in a calculable way upon the peak shape, signal-to-noise ratio, and number of data points

per peak width. Those dependencies are tested by analysis of simulated data. The theory provides estimates for the precision of a *repeated* experiment, based on data from a *single* discrete mass spectrum whose parameters are extracted by least squares fit to a specified line shape. The predictions relate directly to present and potential time-of-flight mass spectrometer performance.

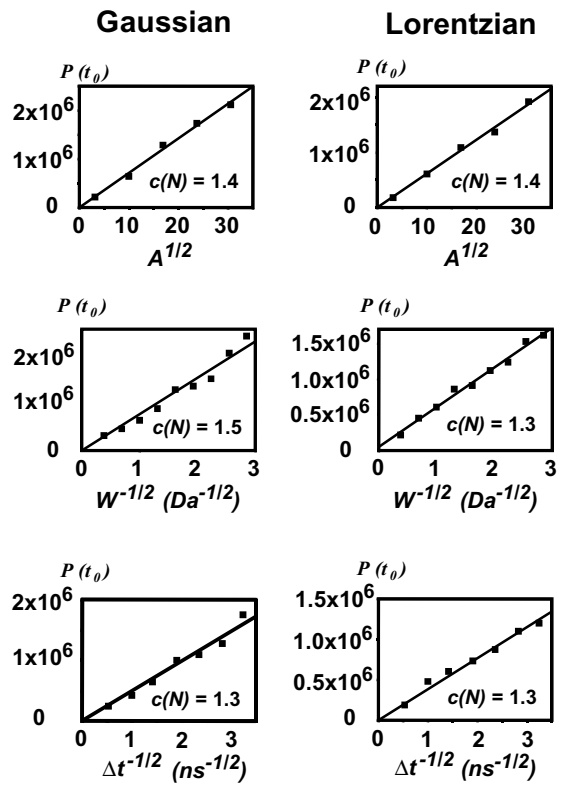

Figure 1. Precision of determination of time of flight, t_0, obtained from simulated time-of-flight (TOF) mass spectra with Gaussian (left) and Lorentzian (right) peak shapes, as a function of peak amplitude A (top), width, W (middle), and data sampling interval, Δt. The data correspond to a 5 kDa ion, initially accelerated to 25 keV kinetic energy, for a flight distance of 2 m. $c(N)$ is obtained from the slope of each line. Top: A dependence, for W = 1 Da (m/Δm = 5000), and Δt = 0.5 ns (2 GHz sampling rate). Middle: W dependence, for A = 100 counts, and Δt = 0.5 ns. Bottom: Δt dependence, for A = 100 counts, and W = 1 Da.

Acknowledgements: This work was supported by the NSF National High Field FT-ICR Facility (CHE-94-13008), Florida State University and the National High Magnetic Field Laboratory in Tallahassee, FL.

[1] Lee, H.-N., *et al.,* Anal. Chem., **72**, 2256-2260 (2000).

Analysis of Electrophoretic Transport of Macromolecules Using Pulsed Field Gradient Nuclear Magnetic Resonance

Locke, B.R., FAMU-FSU College of Engineering, Chemical Engineering
Moerland, T.S., FSU, Biology
Gibbs, S.J., NHMFL/FAMU-FSU CoE-CE
Acton, M., FAMU-FSU CoE-CE

The overall objective of the work performed on this project is to apply pulsed field gradient NMR spectroscopy (PFGNMR) to the analysis of transport by diffusion, electrophoresis, and electro-osmosis in porous media. Electro-osmotic flow is the flow of water induced by an electrical field applied in a medium with fixed surface charges. Electro-osmotic flow in porous media can have an important impact in many environmental and biological systems. MRI is an excellent tool to analyze flow in porous media, because it is not an invasive technique, and it does not require contrast agents or labels (at least for proton imaging).

Magnetic resonance imaging (MRI) has been used to study electro-osmotic flow in a porous medium consisting of spherical glass particles ranging from 2.0 mm to 4.0 mm in diameter. Electrodes placed at each end of a 1 cm glass tube containing the spheres and solution were used to generate flow. Pulsed field gradient MRI at 500 MHz and 600 MHz was used to measure the fluid velocity fields, and provided in-plane image resolution of approximately 78 μm by 78 μm for 100 μm thick slices. Velocity fields as functions of applied voltage were measured for four cases: (1) empty tube with open ends, (2) empty tube with closed ends, (3) tube with packing and closed ends, and (4) tube with packing and open ends.

Systems with the ends of the tubes closed, both with and without particles, showed regions of flow reversal. In the case containing particles, flow reversal occurred over a length scale of approximately the size of a single particle. The standard deviation, or spread of the velocity distribution for the closed tube experiments, scaled approximately linearly with

increasing applied voltage, while the velocity mean remained approximately zero. In the open tube system, both the mean velocity and the standard deviation of the velocity distribution scaled linearly with the applied voltage. Detailed analyses of the velocity distribution histograms indicate that the bundled-capillary tube model of electro-osmotic flow in porous media is not adequate for describing the data.

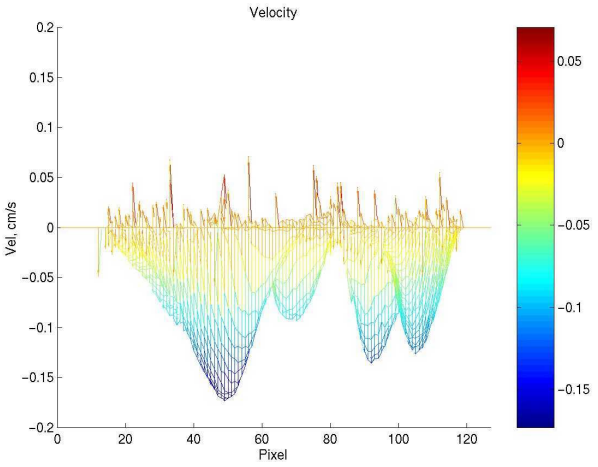

Figure 1. Electroosmotic velocity profile in a porous medium consisting of solid glass spheres. Applied voltage of 25 V with tube ends open to atmospheric pressure.

Acknowledgements: This projected is supported by NASA through grant UGS95-0041.

Solid State Ruthenium NMR Spectroscopy at High Magnetic Field

Ma, Z.R., NHMFL
Zheng, J.P., FAMU-FSU College of Engineering
Fu, R., NHMFL

There are growing interests in studying ruthenium because of its importance in various fields, such as inorganic chemistry, photochemistry, organometallic and coordination complexes, catalytic reactions, and also electrode material. It is known that some ruthenium dihydrogen complexes are active catalysts in hydrogenation and hydrogen transfer reactions. Several mono- and dinuclear ruthenium carbonyl acetate complexes with nitrogen-containing ligands catalyse the hydrogenation of alkenes, alkynes, and ketones in the presence of water and polar solvents. The ruthenium carbonyl-diimine complexes, based on their photochemical and photophysical properties, and also depending on their structure and environment, can be employed to design new functional molecular photonic materials, such as sensitizers, luminophores, photocatalysts, luminescent probes, and sensors.

As a powerful technique, solid state NMR spectroscopy has been widely used to study these materials. A direct observation of Ru would permit us to characterize the role ruthenium plays in these materials. However, until now, only a few ruthenium NMR spectroscopic studies in solution have been conducted. No Ru solid state NMR study has been reported because ruthenium is a low gamma nucleus with a large quadrupole moment leading to an extremely broad resonance peak. High field NMR spectroscopy available at the NHMFL makes such observation possible because the high field significantly enhances the sensitivity and greatly reduces the quadrupole line broadening. Ruthenium has two magnetically active isotopes: ^{99}Ru(I=5/2) and ^{101}Ru(I=5/2). Although the receptivity of ^{99}Ru is only about half of that of ^{101}Ru, it is preferable to observe ^{99}Ru because it possesses a relatively low quadrupole moment compared to ^{101}Ru. Here, we report on the preliminary solid state ^{99}Ru NMR spectroscopic study at high magnetic field.

Fig. 1 shows a ^{99}Ru MAS NMR spectrum of triruthenium dodecacarbonyl ($Ru_3(CO)_{12}$). $Ru_3(CO)_{12}$ is one of the most common starting materials used in the synthesis of ruthenium complexes, and has been known to be an active catalyst applied in many chemical reactions. The isotropic chemical shift of ruthenium disperses over 8300 ppm. In other words, the Ru resonance is extremely sensitive to its chemical environment. Therefore, the high-resolution MAS measurements on ruthenium materials will provide detailed structural information. Recently, we have been focusing on the Ru NMR observation in hydrous ruthenium oxide at high field. It is expected that high resolution Ru NMR spectra will be able to distinguish the Ru valence states and structures at different water content of hydrous ruthenium oxides,[1] which will provide direct information on the relationship

between the proton charge storage, and the structure of hydrous ruthenium oxide.

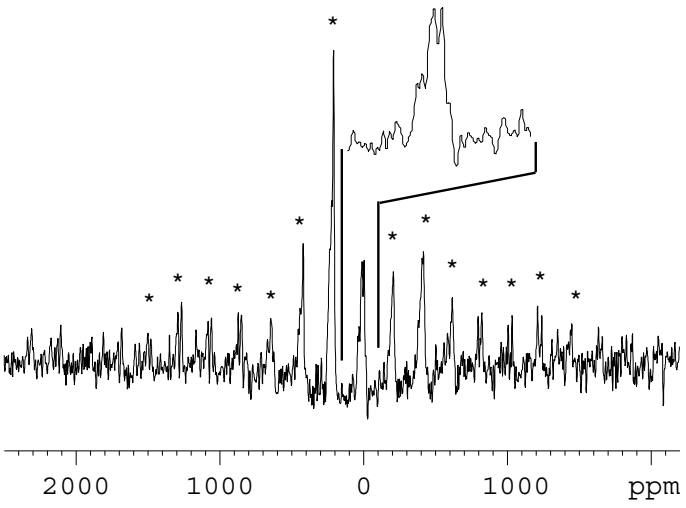

Figure 1. ^{99}Ru MAS NMR spectrum of triruthenium dodecacarbonyl ($Ru_3(CO)_{12}$) at a spin rate of 8 kHz. The spectrum was recorded on a Bruker DRX 833 NMR spectrometer employing a 4 mm homemade MAS probe. The spinning sidebands are indicated by *. The centerband is expanded showing three resonance lines.

[1] Ma, Z.R., *et al.*, Chem. Phys. Lett., **331**, 64-70 (2000).

The Influence of Packing Homogeneity and Distributor Design on Flow Uniformity in Low Pressure Chromatographic Columns Studied by Magnetic Resonance Imaging Velocimetry

◤IHRP◢

Park, J.C., FAMU-FSU College of Engineering/ NHMFL
Raghavan, K., FAMU-FSU CoE/NHMFL
Gibbs, S.J., FAMU-FSU CoE/NHMFL

Flow inhomogeneity and axial development in low pressure chromatographic columns have been studied by magnetic resonance imaging velocimetry with a pulsed field gradient method. The columns studied were all 11.7 mm ID and were packed with 50 µm diameter porous polyacrylamide, 99 µm diameter impermeable polystyrene, or 780 µm diameter impermeable polystyrene beads. All three columns exhibit (1) significant flow non-uniformities at the entrance of the column, caused by poor distributor design or void space at the column entrance, which relax on a length scale of the column radius, and (2) near wall channeling in which flow within a few particle diameters of the wall is substantially larger than flow in the rest of the column for fully developed flow. In addition, the 99 µm bead column exhibits a region extending from about ten particle diameters from the wall to 3 to 5 particle diameters from the wall in which the fully developed flow velocity is substantially less than in other regions of the column. This latter effect is thought to be associated with locally reduced void fraction caused by increased axial stress from wall friction during packing and consolidation and is reproducible for the same column and packing material. An example of the data for the 50 µm bead column is shown in Fig. 1. Better understanding of the origins of these effects may lead to improved distributor and column designs and packing procedures. A manuscript concerning this work has been submitted.

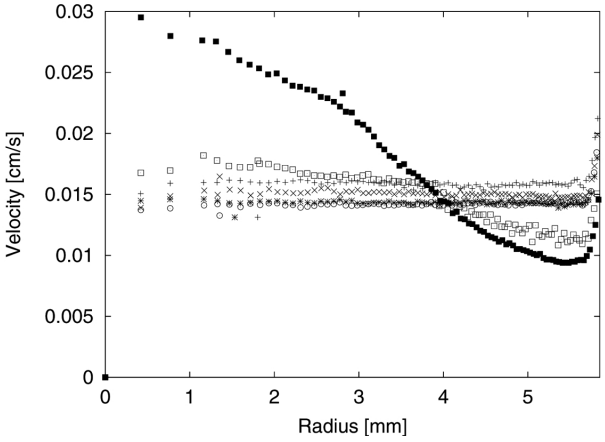

Figure 1: Radial fields of axial velocity showing flow development in the column packed with porous 50 µm diameter polyacrylamide size-exclusion beads. Points represent the average of axial velocities in 200 pixels within a given radial bin. The standard deviation in each bin is approximately 10% of the velocity. The distance of the slices from the entrance distributor are (filled circles): 1mm, (all other symbols) > 4 mm. Flow development is complete within one column radius. All profiles show a strong wall effect.

Acknowledgements: The 500 MHz microimaging NMR spectrometer used for this work was acquired with funds provided by NSF (CTS-9601924), the NHMFL, FAMU, and FAMU-FSU College of Engineering. Work was also supported in part by the NHMFL In-House Research Program.

High Field Transient EPR of Bisadducts of Fullerene C_{60}

Pasimeni, L., Univ. of Padova, Physical Chemistry
van Tol, J., NHMFL
Maniero, A.-L., Univ. of Padova, Physical Chemistry
Brunel, L.-C., NHMFL

As the organic chemistry of fullerenes evolves into more sophisticated molecular architectures with various potential applications, there is an increased need for spectroscopic data for the assignment of structure and function. As the spin-distribution in the excited triplet state is very sensitive to adduct to the C_{60} unit, transient electron magnetic resonance can be an important tool in the assignment. At conventional frequencies, however, only the zero-field splitting parameters and the relative triplet population rates can be obtained. High field EMR increases both field-resolution and time-resolution and enables researchers to obtain the values of the g-tensor components, and in some cases to determine the orientation of the g-tensor with respect to the zero-field splitting (fine-structure) tensor. This enables a finer distinction and a better understanding of the observed differences between different molecules based on the fullerene. The figure shows a transient EPR spectrum at different times after a 532 nm laser pulse of a trans-4 bisadduct of fullerene ($C_{62}(COOEt)_4$)[1] at 50 K. The asymmetric shape is caused by the g-anisotropy, while, the changes of the spectra with time indicate an anisotropy in the relaxation and decay rates as well. These high-field measurements at 240 GHz enable us for the first time to determine the g-anisotropy in this class of compounds.

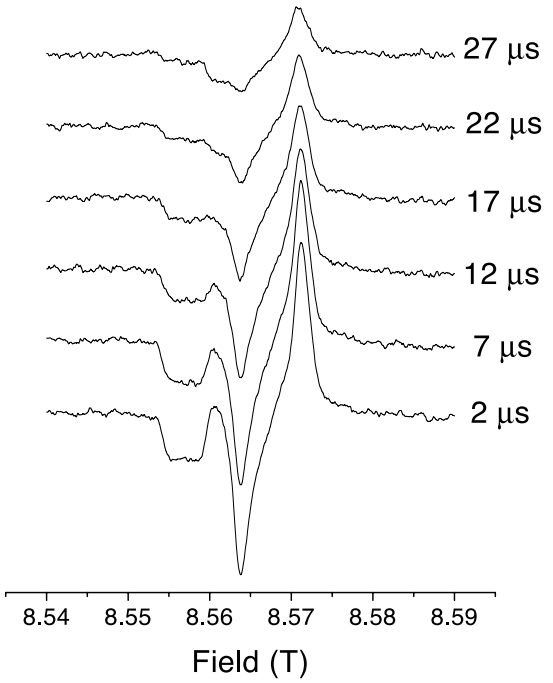

Figure 1. The EPR spectra in the trans-4 bisadduct of $C(COOEt)_2$ with C_{60} at 240 GHz and 50 K after excitation with a laser pulse. The different traces correspond to measurements at different times after the pulse.

Acknowledgements: This work was supported by the NSF under grant CHE-9601731.

[1] Pasimeni, L., *et al*., J. Am. Chem. Soc., **119**, 12896 (1997).

^{17}O Isotropic Chemical Shift Probing of Phase Transitions in Hydrogen-Bonded Solids: Squaric Acid

Pierce, K.L., NHMFL/FSU, Chemistry
Fu, R., NHMFL/FSU, Chemistry
Dalal, N.S., NHMFL/FSU, Chemistry

O-H···O and N-H···O type bonds are known to be involved in ferroelectric phase transitions and other cooperative phenomena shown by a variety of solids, but the underlying mechanisms are not yet well understood. Current theoretical models assume relatively little or no role for the O atom; but, this is perhaps related to the lack of suitable experimental data, in particular, that is obtainable by high resolution NMR. Here, we report our preliminary ^{17}O MAS results on squaric acid, $H_2C_4O_4$, through its paraelectric-antiferroelectric phase transition at 100°C. The data clearly demonstrates that MAS using single crystals provides much (~factor of 4) narrower peaks than with powders, pointing to the role of the anisotropic bulk magnetic susceptibility (ABS) broadening mechanisms.[1] The spectrum consists of four well resolved peaks at $T<T_N$ (~373 K), and coalesces to a singlet above $T>T_N$. Several novel

features are notable, including the coexistence of the spectra from the paraelectric and antiferroelectric phase in a short temperature regime around 373 K, two ^{17}O sites in the paraelectric phase, and the dynamic coalescence of the spectra at 373. The latter is in contrast to earlier NQR results where the coalescence was noted to occur at about 425 K. There is a large change in the ^{17}O istotropic chemical sift at T_N, indicating that the phase transition must involve a displacive component, and not solely the order-disorder behavior as assumed in general.

[1] Klymachyov, *et al.,* Z. Phys. B, **104**, 651, (1997).
[2] Fu, *et al*., J. Phys. Chem., **102**, 8732, (1998).

Reading Chemical Fine Print: Resolution and Identification of 3000 Nitrogen-Containing Aromatic Compounds from a Single Electrospray Ionization Fourier Transform Ion Cyclotron Resonance Mass Spectrum of Heavy Petroleum Crude Oil

Qian, K., ExxonMobil Research and Engineering
Rodgers, R.P., NHMFL
Hendrickson, C.L., NHMFL
Emmett, M.R., NHMFL
Marshall, A.G., NHMFL/FSU, Chemistry

Extra heavy petroleum crude oil (50% of the mixture boils at >566 °C) has been analyzed directly, without prior fractionation, by a high-field (9.4 T) Fourier transform ion cyclotron resonance mass spectrometer coupled to an external micro-electrospray ion source. At an average mass resolving power, ($m/\Delta m_{50\%} \approx$ 50,000), a single wideband (250-1250 Da) mass spectrum exhibited ~5000 resolved peaks with an average mass of 617 Da (e.g., up to 7-10 resolved peaks at each nominal mass). Their elemental compositions were positively identified by accurate mass measurement with an average deviation of less than 1 mDa from each assigned elemental composition. The number of elemental compositions at each nominal mass, the number of sulfur/oxygen atoms in a molecule, and aromaticity each increase with increasing mass.

Based on elemental composition alone, we resolve more than 3000 distinct chemical formulas (excluding ^{13}C isotopic species). Of the 3000 unique elemental compositions, we identify 12 major heteroatomic "classes"; (e.g., molecules containing N, NS, NS_2, NO, NOS, etc.); for the various "classes", we identify more than 100 hydrocarbon "types" (e.g., molecules with the same number of rings plus double bonds); and for each "type", we determine the carbon number distribution (20-80 carbons) to reveal the number of alkyl carbons appended to aromatic rings. The present results represent the most complete chemical characterization ever achieved for such a complex mixture, based on a single experimental data set.

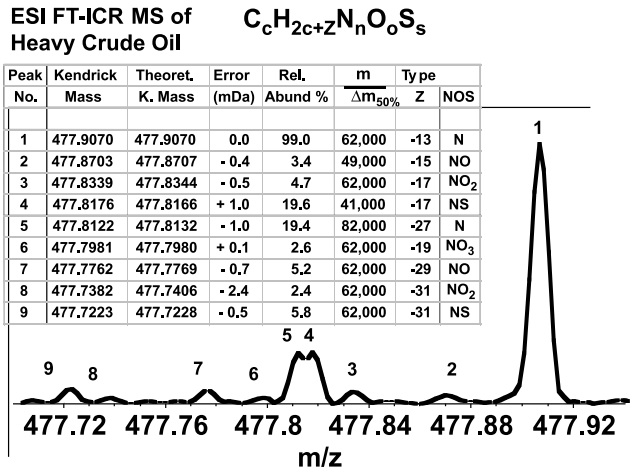

Peak No.	Kendrick Mass	Theoret. K. Mass	Error (mDa)	Rel. Abund %	m $\Delta m_{50\%}$	Type Z	NOS
1	477.9070	477.9070	0.0	99.0	62,000	-13	N
2	477.8703	477.8707	- 0.4	3.4	49,000	-15	NO
3	477.8339	477.8344	- 0.5	4.7	62,000	-17	NO_2
4	477.8176	477.8166	+ 1.0	19.6	41,000	-17	NS
5	477.8122	477.8132	- 1.0	19.4	82,000	-27	N
6	477.7981	477.7980	+ 0.1	2.6	62,000	-19	NO_3
7	477.7762	477.7769	- 0.7	5.2	62,000	-29	NO
8	477.7382	477.7406	- 2.4	2.4	62,000	-31	NO_2
9	477.7223	477.7228	- 0.5	5.8	62,000	-31	NS

Figure 1. Mass scale expanded segment of a full range heavy crude mass spectrum, allowing for resolution and elemental composition assignment (based on accurate mass measurement) of 9 chemically distinct species at a single nominal mass. The tabulated data for the 9 peaks show an average mass error of ~1.5 ppm for the proposed assignments. The chemical "type" (i.e., number of rings plus double bonds) is classified according to "*Z*" value in the chemical formula at the top of the diagram (see text), and the heteroatom content is also shown in the table.

Acknowledgements: The authors thank Daniel McIntosh for machining all of the custom parts required for the 9.4 T instrument construction and John P. Quinn for many helpful discussions. This work was supported by the NSF National High-Field FT-ICR Mass Spectrometry Facility (CHE 99-09502), FSU, and the NHMFL. The authors thank ExxonMobil for supporting this exploratory research of heavy petroleum and the permission to publish the data.

[1] Qian, K., *et al*., "Reading Chemical Fine Print: Resolution and Identification of 3000 Nitrogen-Containing Aromatic Compounds from a Single Electrospray Ionization Fourier Transform Ion Cyclotron Resonance Mass Spectrum of Heavy Petroleum Crude Oil," Energy & Fuels, **15**, 0000-0000 (2001).

Complete Compositional Monitoring of the Weathering of Transportation Fuels Based on Elemental Compositions from Fourier Transform Ion Cyclotron Resonance Mass Spectrometry

Rodgers, R., NHMFL
Blumer, E.N., NHMFL
Freitas, M.A., NHMFL
Marshall, A.G., NHMFL/FSU, Chemistry

We have determined elemental compositions for hundreds of components of diesel fuel, jet fuel (JP-8), and gasoline and characterized each of their chemical compositions before and after artificial "weathering" (i.e., evaporation to a specified fraction of the original weight). An all-glass heated inlet system (AGHIS) coupled to a homebuilt 6.0 T Fourier transform ion cyclotron resonance (FT-ICR) mass spectrometer provides ultrahigh mass resolving power ($m/\Delta m_{50\%}$ > 100,000, in which $\Delta m_{50\%}$ is the full peak width at half-maximum peak height) and sufficiently high mass accuracy (≤0.8 ppm) for unique identification of all chemical components. A 1 μL septum injection of each weathered/unweathered transportation fuel into the AGHIS yields a mass spectrum containing 100-500 peaks, 50-≤ m/z ≤ 300, with as many as 5 peaks (of different elemental composition) at a given nominal mass. Elemental composition assignment of every peak in the mass spectrum of each fuel and its weathered analogs provides a unique chemical "fingerprint" that serves to identify positively the contaminant and quantitate the extent of weathering. Weathered jet and diesel fuels (and gasoline to a lesser extent) exhibit a significant shift in the relative abundance to higher-mass (m/z ≥ 200) species, in accord with prior gas chromatographic (GC) evidence for a shift toward increased retention time with increased degree of weathering.

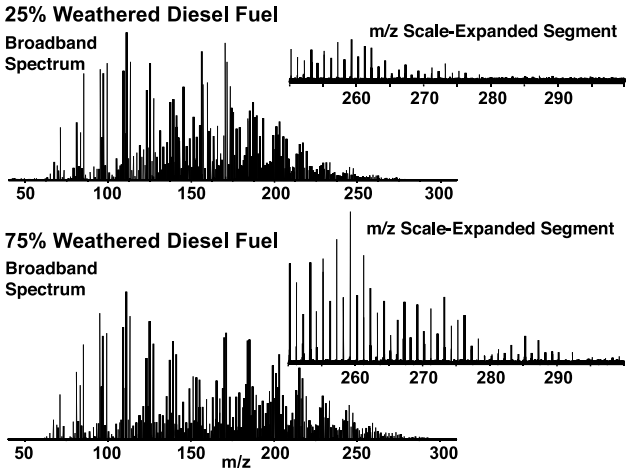

Figure 1. Full-range FT-ICR mass spectra of 25% (top) and 75% (bottom) weathered diesel fuel and mass scale-expanded segments, (250 ≤ m/z ≤ 300) (inset above each broadband spectrum), showing that weathering results primarily in loss of lower-mass species, resulting in a dramatic increase in the relative abundance (and number) of high m/z species. The noise level has been scaled to approximately the same noise level in each zoom mass inset so as to illustrate the increase in relative abundance of species falling between 250 ≤ m/z ≤ 300 as a function of increased weathering.

Acknowledgements: The authors thank Daniel McIntosh for machining all of the custom parts required for the 6 T instrument construction and Randall Pelt for the glasswork on the AGHIS. The authors also thank Christopher L. Hendrickson and John P. Quinn for many helpful discussions and Steve Williams (Eglin AFB) for providing the bulk jet fuel (JP-8). This work was supported by the NSF National High-Field FT-ICR Mass Spectrometry Facility (CHE-94-13008), American Chemical Society Division of Analytical Chemistry graduate fellowship (to RPR) sponsored by the Society of Analytical Chemists of Pittsburgh, FSU, and the NHMFL.

[1] Rodgers, R.P., *et al*., Environ. Sci. Technol., **34**, 1671-1678 (2000).

Compositional Analysis for Identification of Arson Accelerants by Electron Ionization Fourier Transform Ion Cyclotron Resonance High-Resolution Mass Spectrometry

Rodgers, R.P., NHMFL
Blumer, E.N., NHMFL
Freitas, M.A., NHMFL
Marshall, A.G., NHMFL/FSU, Chemistry

Elemental compositions of each of 100 to 500 different constituents (i.e., every peak in a mass-to-charge ratio range, $50 < m/z < 300$) of lighter fluid, kerosene, turpatine, gasoline, diesel fuel, and two brands of mineral spirits (and their weathered analogs) make possible direct identification of each accelerant in a experimental fire, based on electron ionization 6.0 T Fourier transform ion cyclotron resonance (EI FT-ICR) ultrahigh-resolution mass spectrometry. Septum injection of as little as 500 nL of accelerant into an all-glass heated inlet system yields definitive elemental compositions (molecular formulas) based on accurate (< ±1 ppm average error) mass measurement alone. Extraction and EI FT-ICR mass analysis of fire debris from a controlled burn of a couch with simple (lighter fluid) and complex (turpatine) ignitable liquid yielded dozens of elemental compositions serving as a unique "fingerprint" for each petroleum product, despite the presence of up to 249 additional extracted matrix and pyrolysis components. 45 of 56 lighter fluid constituents and 126 of 133 turpatine constituents (not counting ^{13}C-containing species) were identified in the debris from a fire staged for each respective accelerant.

Acknowledgements: The authors thank Daniel McIntosh for machining all of the custom parts required for the 6 T instrument construction and Randall Pelt for glasswork on the AGHIS. The authors also thank Christopher L. Hendrickson, John P. Quinn (National High Magnetic Field Lab) and Carl Chasteen and Carl Lugville (State of Florida Fire and Arson Laboratory) for many helpful discussions.

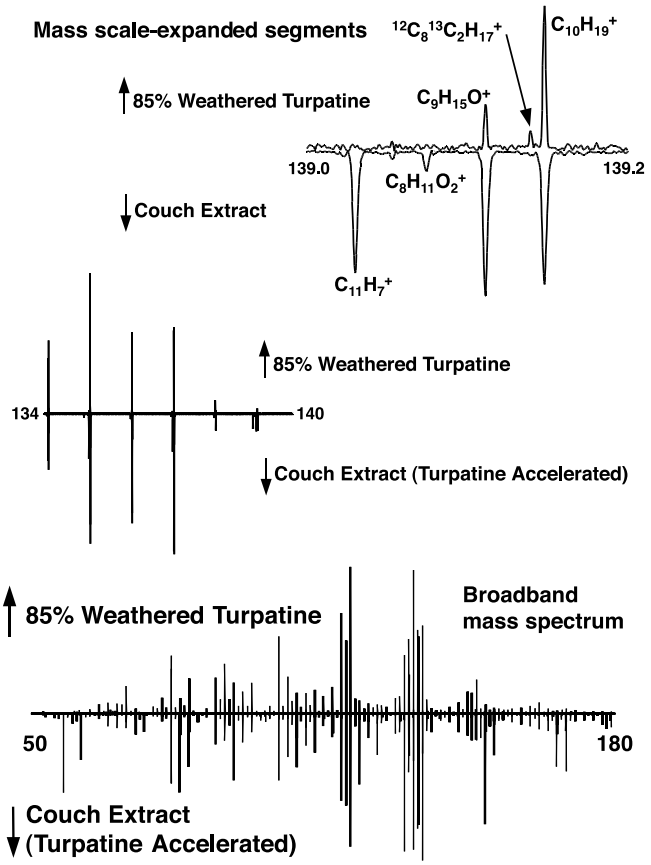

Figure 1. Full-range FT-ICR mass spectrum (bottom) of Soxhlet extracted arson debris collected from a turpatine-accelerated control burn (shown as negative peaks) along with the best match from the arson standard library, namely, 85% weathered turpatine (shown as positive peaks). Both the broadband mass spectra (bottom) and mass scale-expanded segments (middle) illustrate good agreement between the arson extract and library standard. Clinching evidence is provided by mass scale-expended segments such as that near m/z 139 (top). The high resolution and high mass accuracy provided by FT-ICR mass spectrometry allows for peak matching against the arson library even when multiple peaks are present at a nominal mass (e.g.. matrix or pyrolysis products).

[1] Rodgers, R.P., *et al*., "Compositional Analysis for Identification of Arson Accelerants by Electron Ionization Fourier Transform Ion Cyclotron Resonance High-Resolution Mass Spectrometry," J. Forensic Sci., **46**, 0000-0000 (2001).

Molecular Characterization of Petroporphyrins in Crude Oil by Electrospray Ionization Fourier Transform Ion Cyclotron Resonance Mass Spectrometry

Rodgers, R.P., FSU, Chemistry
Hendrickson, C.L., NHMFL
Emmett, M.R., NHMFL
Marshall, A.G., NHMFL/FSU, Chemistry
Greaney, M., ExxonMobil
Qian, K., ExxonMobil

Petroporphyrin compositional analysis of a heavy crude oil has been realized by isolation and subsequent ESI FT-ICR mass spectrometric analysis of the porphyrin-containing fractions. Vanadium octaethyl (V=O(II)OEP) and nickel octaethyl (Ni(II)OEP) porphyrin standards were analyzed to determine favorable electrospray ionization conditions and provide insight as to the molecular species present (e.g., adducts, multimers). Standard V=O(II)OEP and Ni(II)OEP solutions revealed the presence of both monomer and dimer species with a greater relative abundance of monomers. In contrast, mass spectral analysis of a porphyrin fraction from Cerro Negro crude oil was dominated by dimeric species. MS^3 analysis identified a dioctylphthalate (DOP) contaminant, likely introduced during fractionation of the crude oil. DOP-porphyrin complexes and porphyrin-porphyrin dimers were then identified. InfraRed MultiPhoton Dissociation (IRMPD) of dimeric species produced the corresponding monomers with minimal fragmentation. The monomeric petroporphyrins were analyzed to reveal the metal (Ni(II) or V=O(II)), porphyrin type (e.g., etio vs. DPEP), and distribution of alkylation.

Acknowledgements: The authors thank Daniel McIntosh for machining the custom parts required for the 9.4 T instrument construction, and John P. Quinn for his help with instrumental modifications. This work was supported by NSF (CHE-94-13008 and CHE 99-09502), FSU, and the NHMFL. The authors also thank ExxonMobil for permission to publish this data.

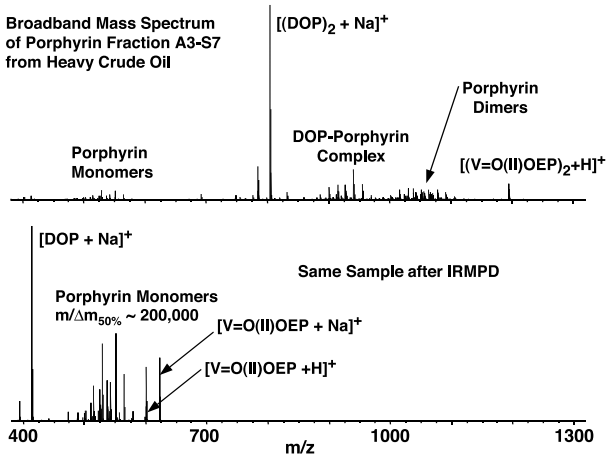

Figure 1. Broadband ESI FT-ICR mass spectrum of A3-S7 fraction isolated as in Fig. 1, shown before (top) and after (bottom) infrared multiphoton dissociation. Top: Three dimer distributions in the range, $800 < m/z < 1100$. The species at m/z 800 was identified by MS^3 experiments as dioctyl phthalate (DOP) dimer. The remaining two dimer distributions were then identified as petroporphyrin:dioctyl phthalate ($900 < m/z < 1000$) and petroporphyrin:petroporphyrin ($1000 < m/z < 1100$) dimers. Bottom: broadband mass spectrum of the same isolated petroporphyrin fraction after IRMPD. IRMPD dissociates the dimers to yield solely monomers. Each spectrum was the result of 20 co-added time-domain transients, and the sample was spiked with V=O(II)OEP as an internal mass calibrant.

[1] Rodgers, R.P., *et al.,* Can. J. Chem., **79**, 0000-0000 (2001).

High Frequency, 220 GHz, CW ENDOR of a Nitroxide Radical with Delocalized Spin Density

Saylor, C.A., NHMFL
Maresch, G.G., NHMFL
van Tol, J., NHMFL
Maniero, A.L., Univ. of Padova, Physical Chemistry
Brunel, L.-C., NHMFL

High Field Electron Nuclear Double Resonance (ENDOR) permits us to use the increase in g-factor resolution of high frequency EPR to map the angular dependence of the hyperfine interactions in a randomly oriented sample with a small g-value anisotropy. Without high field ENDOR, the angular dependence of the hyperfine coupling can only be determined by single crystal experiments.

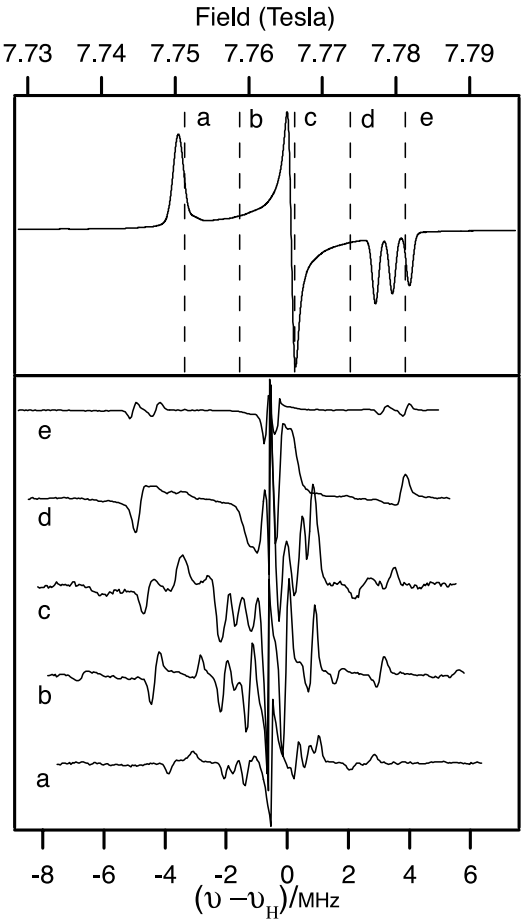

Figure 1. The high field EPR spectra of the indolinone nitroxide radical and the high frequency ENDOR spectra at different resonant fields within the EPR spectra. Microwave Frequency=218.004 GHz, Temperature=5 K.

The aim of this work is to validate the data obtained with the ENDOR spectrometer we built. To do this, we measured the ENDOR spectra of an indolinone nitroxide radical in a polystyrene matrix. The indolinone nitroxide radical belongs to an uncommon group of nitroxide radicals, which are stable both as solids and in solutions, although they have a benzene p system conjugated with an N-O group. The spin density of the nitroxide radical is distributed over a system of eight atoms, with alternating positive and negative signs. This nitroxide radical has been previously studied, using CW EPR and ENDOR at X-band, both in the glassy[1] phase and as a dilute single crystal.[2] These studies determined the proton and nitrogen hyperfine tensors. Therefore, this radical is a good probe to test the ENDOR results obtained at high frequency.

Fig. 1 shows the high frequency ENDOR spectra at the different resonant fields within the EPR spectra. The high frequency ENDOR spectra of the nitroxide along the principal axes have been confirmed with computer simulations starting with the g and A tensors derived from the single crystal studies.2 Further, simulations are currently in progress and will be reported next year. We already know that we have a much better accuracy in the determination of the g and A tensors components. For instance, we can distinguish the contributions from two protons that were assumed identical at X band. Therefore, we conclude that our new ENDOR spectrometer is working very well.

Acknowledgments: We wish to thank A. Sienkiewicz for his help in the early stage of the ENDOR probe development, J. Krzystek for discussion on ENDOR spectroscopy and L. Greci for providing the Nitroxide sample.

[1] Brustolon, M., *et al.*, J. Chem. Soc., Faraday Trans. I, **83**, 69 (1987).
[2] Maniero, A.L., *et al.*, Mol. Phys., **73**, 1 (1991).

EPR from "EPR-Silent" Species: High Frequency and Field EPR Spectroscopy of a Catalytically Relevant Cobalt (I) Molecular Complex

Telser, J., Roosevelt Univ., Chemistry
Krzystek, J., NHMFL
Brunel, L.-C., NHMFL

Initial efforts using high fields and frequencies to yield EPR spectra of "EPR-silent" (integer spin; non-Kramers) complexes of transition metal ions have focused on "early" transition metal ions (broadly defined as groups 3 to 7), specifically chromium[1] and manganese.[2-4] "Late" transition metal ions (groups 8 to 12) have been less investigated, as these often form low-spin complexes, as is always the case for second and third row transition metal ions.

We report here the first use of HF EPR to investigate such an "EPR-silent" non-Kramers system of the quintessential late transition metal, cobalt, specifically as Co^{+} ($3d^8$, S=1) in the complex $CoCl(PPh_3)_3$.[5] This system is of interest for several additional reasons. Although the +1 oxidation state is better known for

cobalt than for any other first row transition metal except copper (and Cu^+, $3d^{10}$, is diamagnetic), Co^+ complexes are nevertheless far less investigated than those of Co^{2+} and Co^{3+}, and most Co^+ complexes have trigonal bi pyramidal geometry and are thus diamagnetic.[6] Furthermore, Co^+ is isoelectronic with the more widely studied ion Ni^{2+}, so that HF EPR of both systems allows one to compare these systems. Analogous complexes of Ni^{2+} are also under investigation by HF EPR, as described in a separate report. Lastly, tetrahedral Co^+ complexes are of direct practical interest. For example, $CoCl(PPh_3)_3$ has been shown by Japanese workers to be an effective catalyst for alkene dimerization and hydrogenation.[7,8]

Fig. 1 presents experimental and theoretical resonant HF EPR fields as a function of frequency for solid $CoCl(PPh_3)_3$. The theoretical lines have been preliminarily calculated by full-matrix solutions of the spin Hamiltonian for an S=1 system. The resulting Hamiltonian parameters are: D=+5.4 cm^{-1}, $|E|$=0.4 cm^{-1}, and g(isotropic)≈2.2. These results will subsequently be refined to account for g anisotropy and will be compared to the structural data available for $CoCl(PPh_3)_3$,[9] which shows a distorted tetrahedral geometry, with approximate C_{3v} point-group symmetry. This distortion leads to a predominantly axial ligand field around Co^+, as reflected in the zero-field splitting parameters. The electronic absorption spectrum of $CoCl(PPh_3)_3$ has also been reported,[5] and it is possible to correlate these data with those obtained from HFEPR to provide a complete picture of the electronic structure of Co^+ in this chemical environment. This analysis requires treatment of the complete $3d^8$ electronic configuration (as a two hole problem), including singlet excited states, which is now possible using software we have developed.

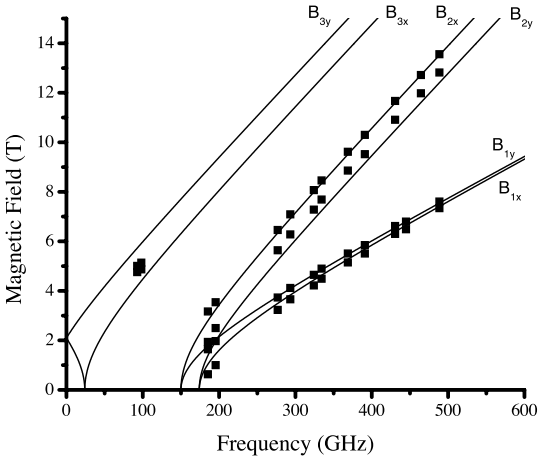

Figure 1. Resonant magnetic field vs. frequency for $CoCl(PPh_3)_3$ as a solid powder at T=5 K. The squares represent experimental points, while the lines represent preliminary theoretical curves for the canonical orientations in the powder spectrum that have been labeled accordingly. The simulation parameters for the plots are: D=+5.4 cm^{-1}, E=+0.4 cm^{-1}, g_{iso}=2.2.

EPR from "EPR-Silent" Species: High Frequency and Field EPR and Magnetic Studies of Nickel(II) Molecular Complexes

Telser, J., Roosevelt Univ., Chemistry
Krzystek, J., NHMFL
Brunel, L.-C., NHMFL
Cao, G., NHMFL

HF EPR studies on complexes of $3d^n$ transition metal ions have emphasized systems with S=2,[1-3] which can occasionally be EPR-visible using conventional spectrometers, when the molecular symmetry is rhombic ($x\neq y\neq z$), as opposed to axial ($x=y\neq z$). Systems with S=1, however, are EPR-silent unless the zero-field splitting is small, or the molecular symmetry is close to cubic ($x=y=z$). Paradigm EPR-silent species are therefore exemplified by distorted octahedral complexes with electronic configuration $3d^2$, such as V(III).[4] However, this situation also results in distorted tetrahedral complexes with electronic configuration $3d^8$, such as Ni(II).

We report here the use of HF EPR to investigate such an EPR-silent, non-Kramers, transition metal ion,

1 Telser, J., *et al.,* Inorg. Chem., **37**, 5769 (1998).
2 Goldberg, D.P., *et al.,* J. Am. Chem. Soc., **119**, 8722 (1997).
3 Barra, A.-L., *et al.,* Angew. Chem. Intl. Ed. Engl., **36**, 2329 (1997).
4 Krzystek, J., *et al.,* Inorg. Chem., **38**, 6121 (1999).
5 Aresta, M., *et al.,* Inorg. Chim. Acta, **3**, 227 (1969).
6 Cotton, F.A., *et al.*, *Advanced Inorganic Chemistry*, 6th ed. (Wiley, 1999) pp 814-835.
7 Kawakami, K., *et al.,* J. Mol. Catal., **5**, 175 (1979).
8 Kanai, H., *et al.,* Bull. Chem. Soc. Jpn., **59**, 1277 (1986).
9 Cassidy, J.M., *et al.,* Acta Crystallogr., **C47**, 2094 (1991).

Ni^{2+} ($3d^8$, S=1), in the complexes $NiX_2(PPh_3)_3$, where X=Cl, Br, I.[5,6] These systems are of interest since, although the 2+ oxidation state is the most common for nickel, most four-coordinate Ni^{2+} complexes have square planar geometry, and are thus S=0. The synthesis of tetrahedral, paramagnetic Ni^{2+} complexes forty years ago was a landmark in coordination chemistry.[5,6] The distorted tetrahedral structure (approximate C_{2v} point-group symmetry) was subsequently confirmed by x-ray crystallography for the chloro,[7] bromo,[8] and iodo[9] complexes. Analogous, isoelectronic complexes of Co^{+} are also under investigation by HF EPR, as described in a separate report. Octahedral complexes of Ni^{2+} with axial distortion are also paramagnetic, and are much more common than tetrahedral complexes. A representative system has been studied successfully by HF EPR at the NHMFL as well.[10]

All three halo complexes have been investigated by HF EPR. Fig. 1 presents experimental and theoretical resonant field vs. operating frequency dependencies for solid powder $NiCl_2(PPh_3)_2$ at 5 K. Signals due to all of the expected branches can be observed at the appropriate frequencies. The theoretical lines have been calculated by full-matrix solutions of the spin Hamiltonian for an S=1 system. The resulting Hamiltonian parameters are: D=+13.3 cm^{-1}, $|E|$=1.8 cm^{-1}, and g_x=2.15, g_y=2.20, g_z=2.20. In a similar way, the parameters found $NiBr_2(PPh_3)_2$ were: D=+4.2 cm^{-1}, $|E|\approx$1.4 cm^{-1}, and $g\approx$2.20. No HF EPR signals were observed for $NiI_2(PPh_3)_2$. This complex was investigated by variable temperature magnetic susceptibility, which showed $|D|\approx$30 cm^{-1}, $|E|\approx$5 cm^{-1}, and $g\approx$2.00, again using a full-matrix solution to the spin Hamiltonian with non-linear least-squares fitting. Zero-field splitting this large causes $NiI_2(PPh_3)_2$ to be indeed EPR-silent, even at frequencies up to 550 GHz.

The wide range of zero-field splitting parameters in the $NiX_2(PPh_3)_3$ complexes is unexpected given that their solid state structures are quite similar.[7-9] Electronic absorption data for these compounds has not been reported, but will be obtained and correlated with HF EPR data to provide a better understanding of the electronic structure of Ni^{2+} in this chemical environment. This analysis requires treatment of the complete $3d^8$ electronic configuration (as a two hole problem), including singlet excited states, which is now possible using software we have developed.

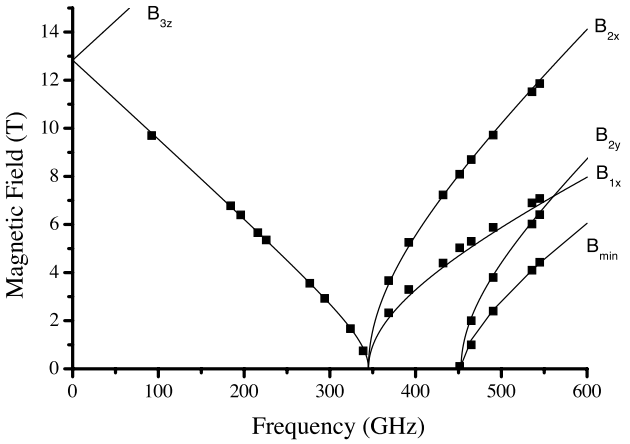

Figure 1. Resonant magnetic field vs. operating frequency for $NiCl_2(PPh_3)_2$ as a solid powder at 5 K. Solid squares represent the experimental points, and the lines represent theoretical curves for the canonical transitions as indicated by the labels. The simulation parameter set for the plots is: D=+13.3 cm^{-1}, E=+1.8 cm^{-1}, and g_x=2.15, g_y=2.20, g_z=2.20.

1 Telser, J., *et al.,* NHMFL 1999 Annual Research Review, and concurrent.
2 Telser, J., *et al.,* Inorg. Chem., **37**, 5769 (1998).
3 Krzystek, J., *et al.,* Inorg. Chem., **38**, 6121 (1999).
4 Barra, A.-L., *et al.,* Angew. Chem. Intl. Ed. Engl., **36**, 2329 (1997).
5 Venzani, L.M., J. Chem. Soc., 719 (1958).
6 Garton, G., *et al.,* J. Chem. Soc., 3625 (1963).
7 Brammer, L., *et al.,* Acta Cryst., **C45**, 400 (1989).
8 Jarvis, J.A.J., *et al.,* J. Chem. Soc. A, 1473 (1968).
9 Humphry, R.W., *et al.,* Acta Cryst. A, **44**, 1717 (1988).
10 Pardi, L.A., *et al.,* Inorg. Chem., **39**, 159 (2000).

EPR from "EPR-Silent" Species: High Frequency and Field EPR Spectroscopy of Vanadium (III) Molecular Complexes

Telser, J., Roosevelt Univ., Chemistry
Krzystek, J., NHMFL
van Tol, J., NHMFL
Brunel, L.-C., NHMFL

In our continuing quest to characterize all "EPR-silent" integer-spin transition metal ions, we have performed a series of experiments on V^{3+}($3d^2$,

S=1), in the following complexes: $V(acac)_3$, $VBr_3(thf)_3$, and $VCl_3(thf)_3$, where acac and thf are 2,4-pentanedionate (acetylacetonate, a chelating ligand) and tetrahydrofuran, respectively. These systems are of specific interest as relatively rare examples of stable vanadium(III) complexes, but given that $3d^2$, S=1 complexes are quite uncommon, they are of general interest as well. Furthermore, our efforts thus far on "EPR-silent" integer-spin systems have emphasized those with S=2,[1-4] which can sometimes be EPR-visible using conventional spectrometers when the molecular symmetry is rhombic ($x \neq y \neq z$), as opposed to axial ($x=y \neq z$). Systems with S=1, however, are always EPR-silent at conventional frequencies unless the zero-field splitting is small, or molecular symmetry is close to cubic ($x=y=z$). Thus, the S=1 systems study is important in demonstrating the breadth of applicability of the HFEPR technique.

We have previously reported on one of the presently investigated complexes, $V(acac)_3$,[5] but faced a need to re-interpret the results due to inconsistencies in the fit parameters necessary to simulate the experimental spectra. A new set of spectra was therefore taken. The spin Hamiltonian parameters obtained for the three complexes under study are shown in Tab. 1. It is worth noting that in at least two of the three systems, the zfs tensor is strongly rhombic, including the re-evaluated $V(acac)_3$. The $V(acac)_3$ parameters agree reasonably well with the older susceptibility measurements,[6] while (a) improving them, and (b) adding the rhombicity parameter E that was not measured by susceptibility. In the case of $VCl_3(thf)_3$, the zfs tensor is most likely rhombic as well; however, the data is incomplete as yet to confirm this fact. HFEPR data is combined with earlier electronic absorption data to provide a full picture of the electronic structure of V^{3+} in the chemical environment as studied. This analysis requires treatment of the complete $3d^2$ electronic configuration, including singlet excited states.

Complex	D (cm^{-1})	E (cm^{-1})	g_x	g_y	g_z
$V(acac)_3$	7.50(5)	2.0(1)	1.80(5)	1.80(5)	1.9(1)
$VBr_3(thf)_3$	10.2(1)	2.7(1)	1.80(5)	1.80(5)	1.6(1)
$VCl_3(thf)_3$	12 ± 4	0 - 4			

Table 1. Spin Hamiltonian parameters used in simulating the experimental spectra of the three V^{3+} complexes under study.

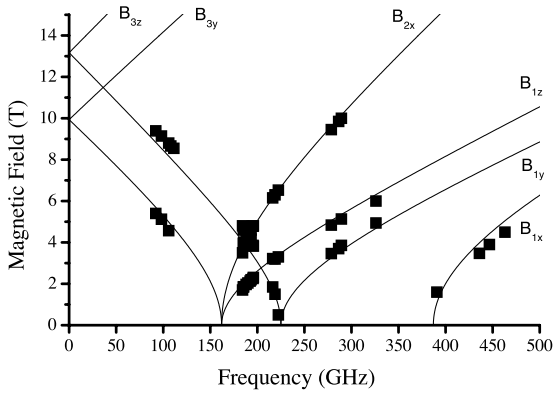

Figure 1. Resonant field vs. frequency dependencies of HFEPR transitions in solid $VBr_3(thf)_3$ at T=5 K. The squares are experimental points, and their size approximates the experimental error. The theoretical lines have been calculated by full-matrix diagonalization solutions of the spin Hamiltonian for an S=1 system, using spin Hamiltonian parameters listed in Tab. 1. The particular transition branches are identified and labeled accordingly. Those branches which are undetectable have been omitted in the simulations for the sake of clarity.

1 Goldberg, D.P., *et al.*, J. Am. Chem. Soc., **119**, 8722 (1997).
2 Barra, A.-L., *et al.*, Angew. Chem. Intl. Ed. Engl., **36**, 2329 (1997).
3 Telser, J., *et al.*, Inorg. Chem., **37**, 5769 (1998).
4 Krzystek, J., *et al.*, Inorg. Chem., **38,** 6121 (1999).
5 Telser, J., *et al.,* 1999 NHMFL Annual Research Review.
6 Gregson, A.K., *et al.*, Inorg. Chem., **17**, 1216 (1978).

Lowest Excited Triplet State in Porphyrins Studied by High Field Transient EMR

van Tol, J., NHMFL
Angerhofer, A., UF, Chemistry
Brunel, L.-C., NHMFL

The porphyrin molecule is a basic unit of many biologically important systems like hemoglobin, chlorophyll, and other cofactors that play a role in photosynthesis. As we are engaged in measuring these biological systems with high field transient EMR, we are currently investigating some model systems based on the porphyrin unit with different central metal ions and side groups.

Our results show that high frequency delivers valuable information about the Zeeman splitting in the lowest excited triplet state, which cannot be resolved at lower frequencies. From simulations of spectra obtained at different frequencies, we can also obtain information on the relative orientations of the g-tensor with respect to the zero-field axes. The figure shows a spectrum of a solid solution of (free-base) tetra-phenyl porphyrin (TPP) in polystyrene at 240 GHz. The positive and negative components in the absorption spectra correspond to complementary emission and absorption components between the triplet levels, which have a non-equilibrium population distribution after the excitation. This spectrum represents the first transient EPR spectrum measured at frequencies above 100 GHz. The shift to low field of the central peaks with respect to the outer peaks is due to the g-anisotropy, and though the anisotropy is small, it is well resolved at these frequencies (g_{xx}-g_{zz}=16.3(3)·10^{-4}, g_{yy}-g_{zz}=8.3(3)·10^{-4}). These and other results in a variety of other porphyrin based systems will enable a better interpretation of the results obtained in porphyrin-based biological systems.

Acknowledgements: This work was supported by the NSF under grant CHE-9601731.

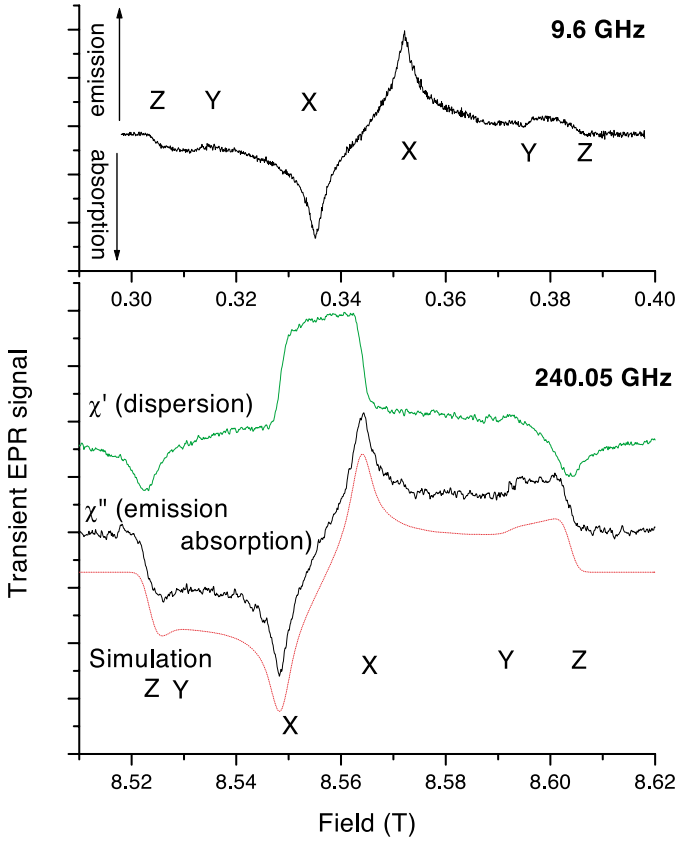

Figure 1. Transient EPR spectra of TPP in polystyrene at X-band (top), and at 240 GHz (bottom), taken at 290 and 170 K resp. The X, Y, and Z labels indicate the spectral positions corresponding to the magnetic field oriented along the zero-field splitting axes. The asymmetry of the 240 GHz spectra is due to g-anisotropy.

Direct Optical Spectroscopy of Gas-Phase Molecular Ions Trapped and Mass-Selected by Ion Cyclotron Resonance: Laser-Induced Fluorescence Excitation Spectrum of Hexafluorobenzene ($C_6F_6^+$)

◤IHRP◢

Wang, Y., NHMFL
Hendrickson, C.L., NHMFL
Marshall, A.G., NHMFL/FSU, Chemistry

The laser-induced fluorescence excitation spectrum of gas-phase hexafluorobenzene cations ($C_6F_6^+$) has been measured at room temperature, by ion trapping and cyclotron frequency-based mass selection.[1] The optical spectral resolution, vibrational state assignments, and their corresponding wavelengths compare favorably to prior data (V. E. Bondybey and

T. A. Miller, *J. Chem. Phys.*, **1979**, *70*, 138-146). The present approach offers a general entry into optical spectroscopy of collisionally stable gas-phase ions.

LIF spectra have been obtained previously for dozens of organic ions, at much higher resolution, in either supersonic jets or inert gas matrices. However, the present approach offers several unique advantages: (a) It offers general entry to optical spectroscopy of any collisionally stable gas-phase ion: e.g., positive or negative ions, molecular ions or fragments, odd- and even- electron ions, produced by virtually any ionization method. (b) Ion fluorescence is detected in the absence of any fluorescent neutrals. (c) Ion fluorescence is detected in the absence of ions of any other mass-to-charge ratios. (d) For gas-phase radical ions, the present approach should make possible optically detected electron magnetic resonance, previously demonstrated for atomic (but not yet for molecular) ions. (e) Fluorescence energy transfer could determine the point-to-point distance between donor and acceptor groups, for the most direct determination of gas-phase biomacromolecular conformation.

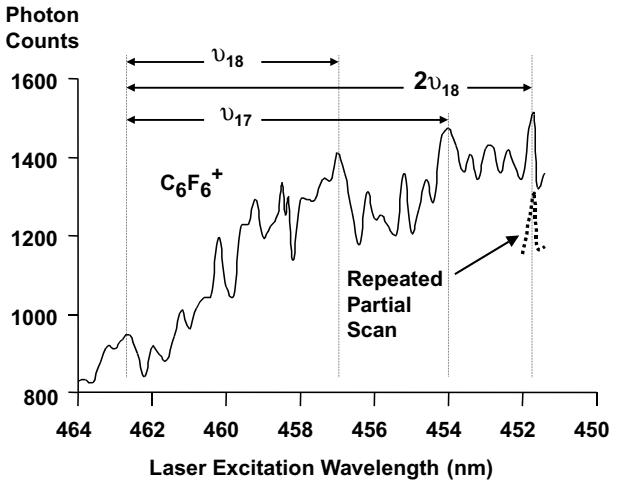

Figure 1. LIF excitation spectrum of $C_6F_6^+$ ions, mass-selected according to their ion cyclotron resonance frequency and Penning-trapped at 3 T. A single peak represents a repeated measurement over part of the spectral range.

Acknowledgements: We thank Jared J. Drader, John P. Quinn, Hak-No Lee, Guo-Zhong Li, and Dan McIntosh for helpful advice and assistance. This work was supported by NSF (CHE-99-09502), FSU, and by an NHMFL In-House Research Grant.

[1] Wang, Y., *et al*., "Direct Optical Spectroscopy of Gas-Phase Molecular Ions Trapped and Mass-Selected by Ion Cyclotron Resonance: Laser-Induced Fluorescence Excitation Spectrum of Hexafluorobenzene ($C_6F_6^+$)," Chem. Phys. Lett., **000**, 0000-0000 (2000).

Mass-Selective Ion Accumulation and Fragmentation in a Linear Octopole Ion Trap External to a Fourier Transform Ion Cyclotron Resonance Mass Spectrometer

Wang, Y., NHMFL
Shi, S.D.-H., NHMFL
Hendrickson, C.L., NHMFL
Marshall, A.G., NHMFL/FSU, Chemistry

Electrosprayed protein ions are accumulated and mass-selected in an external linear octopole trap before injection into a Fourier transform ion cyclotron resonance mass spectrometer. Mass selection is performed by application of superimposed rf and dc octopole electric potentials during ion accumulation. Ion trajectory stability and mass selection in the octopole field are explained qualitatively by analogy to a quadrupole mass filter. Accumulation of ions from a selected m/z range is demonstrated experimentally for 7 T and 9.4 T ESI FT-ICR mass spectrometers. Ion fragmentation in the octopole may occur under certain operating conditions.

Acknowledgements: We thank John P. Quinn and Dr. Mark R. Emmett for technical assistance. This work was supported by NSF (CHE-93-22824 and CHE-94-13008), FSU, and the NHMFL.

[1] Wang, Y., *et al.*, Int. J. Mass Spectrom., **198**, 113-120 (2000).

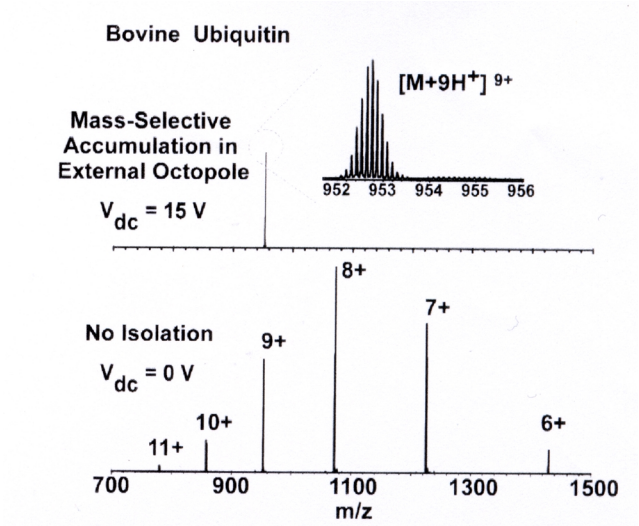

Figure 1. External accumulation and m/z-selection of electrosprayed bovine ubiquitin charge states, observed by 9.4 T FT-ICR MS. Top: External octopole ion trap operating conditions: $\omega/2\pi$ =1.5 MHz, V_{rf} = 142 $V_{0\text{-}p}$. Top: V_{dc} = 15 V. Bottom: rf-only octopole potential field (V_{dc} = 0 V)

An NMR Investigation of Peptide Inhibitors for HIV-1 Protease

West, J., FAMU, Chemistry
Smith, T., FAMU-FSU College of Engineering
Dunn, B.M., UF, Biochemistry and Molecular Biology

A major difficulty in the development of inhibitors for HIV-Protease has been the rapid mutations in the viral genome that results in resistance to the drug through changes in the protein target. Moreover, many resistant mutations can occur distant from the active site. These observations support a mechanism for drug resistance that is not specific to each inhibitor structure. Rather, they support a mechanism that affects a dynamic process of protease closure and conformation change upon ligand binding. Thus, any design for the protease inhibitor should account for the dynamic process that occurs upon ligand binding. It should induce a conformation in the protease that is not affected by point mutations.

We designed peptide inhibitors of HIV-protease that address the dynamics of the mutations in this protein. These inhibitors have a "reduced" peptide bond and a phenylalanine group in the middle, and a naphtylalanine on either end. We have acquired NMR spectra and are analyzing the relative flexibilities of these peptides. On the one hand, some flexibility is good in that the peptide can adapt to the active site of the enzyme in its open conformation. On the other hand, too rigid a peptide inhibitor will reduce the population of the best conformer and will be less able to adapt to the point mutations in the protease that affects its dynamics. The data accumulated in this investigation will lay the groundwork for examining the effect that these inhibitors have on the dynamics of the protease at a future date.